# Numerical Simulation of Laminar Reacting Flows Using Unstructured Finite Volume Method With Adaptive Refinement

**Sung-Mo Kang, Hoo-Joong Kim and Yong-Mo Kim**
Department of Mechanical Engineering,
Hanyang University,
Seoul 133-791, KOREA

## ABSTRACT

A pressure-based, unstructured finite volume method has been applied to couple the chemical kinetics and fluid dynamics and to capture effectively and accurately the steep gradient flame field. The pressure-velocity coupling is handled by two methodologies including the pressure-correction algorithm and the projection scheme. A stiff, operator-split projection scheme for the detailed nonequilibrium chemistry has been employed to treat the stiff reaction source terms. The conservative form of the governing equations are integrated over a cell-centered control volume with collocated storage for all transport variables. Computations using detailed chemistry and variable transport properties were performed for two laminar reacting flows: a counterflow hydrogen-air diffusion flame and a lifted methane-air triple flame. Numerical results favorably agree with measurements in terms of the detailed flame structure.

**Keywords** : unstructured grid, finite volume method, finite-rate chemistry, variable transport properties, triple flame.

## INTRODUCTION

Combustion is a special type of physical phenomenon that encompasses fluid dynamics, chemical thermodynamics, chemical kinetics, and heat transfer. The combustion processes are characterized by the presence of multiple, vastly differing time and length scales, as well as flow-speeds at wide variation of Mach numbers. The chemical time scale itself is broken up into widely varying time scales, i.e., disparate reaction rates, and the numerical solution is dominated by the species that have the fastest reaction rates or smallest time scales. Such a system is termed "stiff" and result in a set of coupled nonlinear stiff partial differential equations. Thus, successful analysis of fluid flow accompaning chemical reaction depends on stability and accuracy of the numerical scheme coupling the chemistry with fluid dynamics, robustness of the solution algorithm used to solve the

governing transport equations, and reaction mechanism used to account for the detailed chemical kinetics. And in order to properly resolve the flame front structure and to account for the multiple-length scales, the grid points must be placed where steep gradients exist and must move with the flame front if the problem is time-dependent.

This study has been mainly motivated to develop and validate a numerical tool which can couple the chemical kinetics and fluid dynamics and can analyze the precise structures and stabilization mechanism of finite-rate reacting flows such as triple flames with locally higher gradients, using highly non-uniform cell distributions. To this end, a pressure-based, unstructured-grid Navier-Stokes flow solver were developed and a finite-rate chemisty model has been incorporated, which can achieve both geometric flexibility and solution adaptation to the regions of higher gradient in reacting flows and thus help to capture effectively and accurately the steep gradient flame field. The pressure-velocity coupling is handled by using a SIMPLE family pressure-correction algorithm[1,2] and a projection scheme[3,4]. Together with a conventional operator splitting procedure[5,6], a stiff, operator-split scheme[4] for finite-rate chemistry is employed to overcome the difficulties associated with stiffness due to the disparate time scales.

## NUMERICAL METHOD

### Governing Equations

For a reacting flow that involves a number of species $N$, the governing conservation equations of mass, momentum, and energy can be written in a Cartesian tensor form:

$$\frac{\partial \rho}{\partial t} + \frac{\partial \rho u_k}{\partial x_k} = 0 \tag{1}$$

$$\frac{\partial \rho u_i}{\partial t} + \frac{\partial \rho u_j u_i}{\partial x_j} = -\frac{\partial p}{\partial x_i} + \frac{\partial t_{ij}}{\partial x_j} \tag{2}$$

where $\rho$ is the density, $u_i$ is $i$th Cartesian component of the velocity, $p$ is the static pressure, and $t_{ij}$ is the shear stress tensor,

$$t_{ij} = 2\mu\left(S_{ij} - \frac{1}{3} S_{kk}\delta_{kk}\right),$$
$$S_{ij} = \frac{1}{2}\left(\frac{\partial u_i}{\partial x_j} + \frac{\partial u_j}{\partial x_i}\right) \tag{3}$$

with $\mu$ being the viscosity and $\delta_{ij}$ is the Kronecker delta. The energy equation for static enthalpy $h$, is written as:

$$\frac{\partial \rho h}{\partial t} + \frac{\partial \rho u_j h}{\partial x_j} = \frac{\partial}{\partial x_j}\left(\frac{k}{Cp}\frac{\partial h}{\partial x_j}\right) + \frac{Dp}{Dt} + t_{ij}\frac{\partial u_i}{\partial x_j} + \frac{\partial}{\partial x_j}\left[\frac{k}{C_P}\sum_{i=1}^{N}\left\{\left(\frac{1}{Le_i} - 1\right)h_i\frac{\partial Y_i}{\partial x_j}\right\}\right] \tag{4}$$

where $k$ is the thermal conductivity, $c_p$ is the specific heat of the mixture, $h_i$ is the average enthalpy associated with species $i$, and $Y_i$ is the mass fraction for which the conservation equation of mass takes the form

$$\frac{\partial \rho Y_i}{\partial t} + \frac{\partial \rho u_j Y_i}{\partial x_j} = \frac{\partial}{\partial x_j}\left(\rho D_{i\text{-}N_2}\frac{\partial Y_i}{\partial x_j}\right) + \omega_i \tag{5}$$

where the mass production rate of species $i$, $\omega_i$ is determined from a reaction mechanism for multistep reversible reactions that will be presented below. The transport property $D_{i\text{-}N_2}$ is the diffusion coefficient for diffusion through the species $i$ present in the excess species $N_2$ and $Le_i$ is the Lewis number of the species $i$, defined as

$$Le_i = \frac{k}{\rho c_p D_{i-N_2}} \tag{6}$$

## Discretization on a Cell-entered Control Volume

An advantage of the control volume formulation is the ability to treat complex geometry and physics in a simple and clear fashion. As will be described below, in almost all cases, the basic operations of the calculation of areas, volumes, or fluxes can be accomplished with the use of vector algebra and calculus, which is a physically transparent method for the representation of processes in continuous media. The computational domain is identified and divided into many volume cells as illustrated in Fig. 1. All transport variables are stored at cell centers.

By integrating and also using the divergence

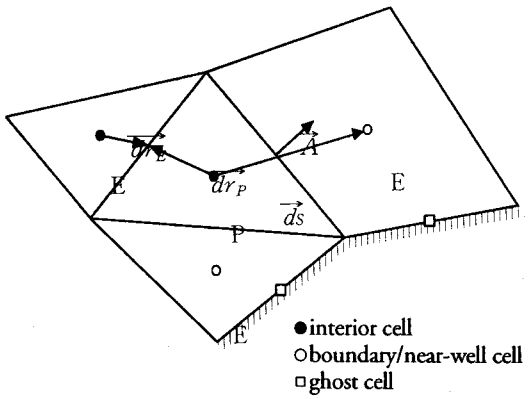


Figure. 1 A representative cell-centered control volume for 2-D unstructured grids, with all necessary geometric vectors and nomenclature

theorem, the $\phi$-transport equation can also be written in integral form as

$$\frac{\partial}{\partial t}\int_\Omega \rho\phi d\Omega = \int_A \vec{F}\cdot\vec{n}dA + \int_\Omega S_\phi d\Omega \tag{7}$$

where $\Omega$ is the domain of interest and $A$ is the surrounding surface; $\vec{n}$ is the directional cosine of $A$ in outward direction. The flux function $\vec{F}$ contains the inviscid and the diffusion flux vector

$$\vec{F} = -\rho\vec{u}\phi + \Gamma_\phi\nabla\phi \tag{8}$$

With the discretization of the spatial domain, the finite volume formulation of flux integral can be evaluated by the summation of the flux vector over each face $f$ of a cell

$$\int_A \vec{F}\cdot\vec{n}dA = \sum_{f=1}^{NB}\left[-(\rho\vec{u}\cdot\vec{n})\phi_f + (\Gamma\nabla\phi\cdot\vec{n})_f\right]$$

$$A_f = \sum_{f=1}^{NB}\left(-J_f\phi_f + D_f\right) \tag{9}$$

where $NB$ is the total surface number for cell P. As shown in Figure 1, at a interface $f$ between cells P and E, the diffusion term can be approximated based on finite difference expressions for the covariant (contravariant) tangent vectors and metric tensors in a curvilinear system, as

$$D_f = \Gamma_f\left[\tilde{\nabla}\phi\cdot\alpha\hat{s} + \overline{\nabla\phi}\cdot(\vec{n}-\alpha\hat{s})\right]A_f \tag{10}$$

$$\tilde{\nabla}\phi\cdot\alpha\hat{s} = \alpha\frac{(\phi_E-\phi_P)}{ds},\ \hat{s} = \frac{\vec{ds}}{ds} \tag{11}$$

$$\overline{\nabla\phi} = (1-gp)\nabla\phi_P + gp\nabla\phi_E,\ gp = \frac{dr_P}{dr_P+dr_E} \tag{12}$$

where $gp$ is a distance-weighted averaging factor and $\alpha$ is a correction coefficient, given as $\alpha = 1/(\vec{n}\cdot\hat{s})$[5].

The interface values, $\phi_f$ and $\overline{\nabla\phi}$ are interpolated from the values at neighbor cells E and P using Eq.(12) while the interface pressure $p_f$ is calculated by averaging the reconstructed face pressure from the neighbor cells, as

$$\int \frac{\partial p}{\partial x_i} d\Omega \approx \nabla p \Omega = \sum_f p_f A_i \tag{13}$$

$$p_f = \frac{1}{2}\left[\left(p_r + \nabla p_r \cdot \vec{dr_P}\right) + \left(p_E + \nabla p_E \cdot \vec{dr_E}\right)\right] \tag{14}$$

The pressure-velocity coupling is handled by using a SIMPLE family pressure-correction algorithm[1,2] and a projection scheme[3,4]. The preconditioned Bi-CGSTAB as well as Point Gauss-Seidel matrix solver is used to solve the final set of linear algebra equations which consist of a nonsymmetric sparse matrix system.

### Thermodynamic Model and Detailed Chemical Kinetics

The viscosity and thermal conductivity of individual species are estimated by employing Chapman-Enskog collision theory and then those for a mixture are determined using the Wilke semiempirical formula. Chapman-Enskog theory and Lennard-Jones potentials are used to estimate the binary-diffusion coefficient between each species and nitrogen[13].

A finite-rate chemistry model is employed to account for the detailed chemical kinetics in a multicomponent reacting system. This study employs a finite-rate chemistry based on a detailed 9 species and 21 elementary reaction steps[6,14] for a hydrogen flame, and 17 species and 51 elementary reaction steps[15] for a methane flame.

An operator-splitting procedure separating the chemical kinetics terms from the fluid dynamics has been employed. This procedure avoids to solve a set of nonlinear stiff partial differential equations due to widely disparate chemical time scales and so improves numerical stability and efficiency.

## RESULT AND DISCUSSION

### Counterflow Nonpremixed $H_2$-Air Diffusion Flame

This counterflow configuration is identical to that studied by Trees *et al.*[7]. The counterflow burner consist of two opposing nozzles with 22.2 mm inner diameter and the distance between nozzles is 12 mm. The aspect ratio, defined as the ratio of the exit diameter of the nozzles to their separation distance, is about 2. The same reaction mechanism comprising 9 species and 21 elementary reaction steps as that in publications[6,14] is used. Computations are made for 20% hydrogen by volume in the fuel stream and undiluted air in the oxidizer stream. The flame is ignited by a heat source with a peak temperature of 2000 K located at the center of mixing layer formed after cold flow mixing of reactants. To test the grid dependency of a solution, two grid systems slightly different from the level of adaptation to the thin flame zone are used. The dense grid has the cells increased about 30% (3160 to 4215). Figure 2 illustrates an unstructured grid with less adaptation and the boundary conditions of the gaseous reactant streams. Here, npoin, ncell, nface, and nfa2 denote the total number of the grid points, control volumes, control faces, and control faces contacting boundaries, respectively.

Figure 3 shows results of the heat release rate, temperature distribution, and velocity vector field, respectively. It can be seen that the diffusion flame has a narrow reaction zone in the mid of the mixing layer.

Figure 4 shows comparisons between the experimental measurements and the numerical calculations of the profiles of temperature and mass fractions of $H_2$, $O_2$, $N_2$, and $H_2O$ along the centerline of nozzles. Figures show

that the calculated profiles agree well with measurements and the stiff projection scheme

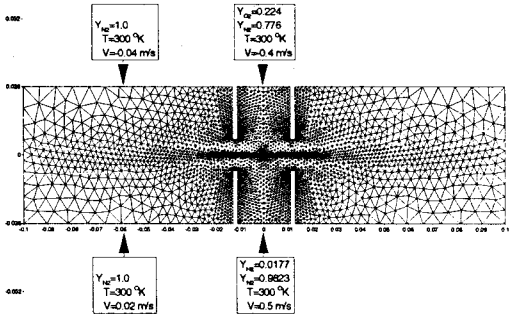


Figure 2 Unstructured grid and boundary conditions for counterflow nonpremixed hydrogen-air diffusion flame (npoin=1678, ncell=3160, nface=4643, nfa2=194).

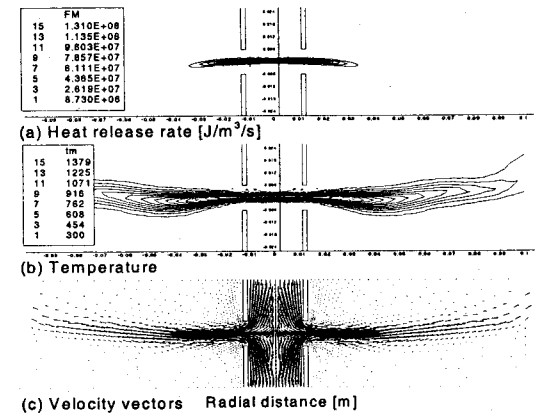


Figure 3 Contours of the heat release rate and temperature distributions, and velocity vectors.

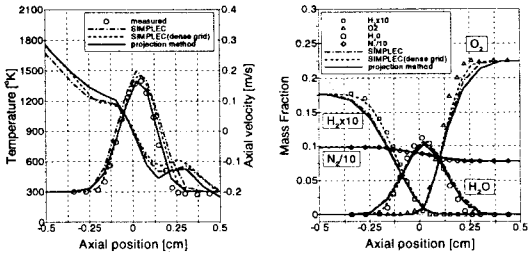


(a) (b)

Figure 4 Comparisons between the measured and calculated profiles of (a) temperature and axial velocity, (b) mass fractions of $H_2$, $O_2$, $N_2$, and $H_2O$ along the centerline of nozzles.

employed here has same accracy as that of implicit scheme. It is also found that a solution dependency on grid refinements appears and the accuracy of predictions is improved for more dense grid.

### Lifted $CH_4$-Air Triple Flame

This laminar flame is studied experimentally and numerically by Plessing *et al.*[8]. They conducted detailed study for a flame with distinct triple flame stucture at the leading edge and a low lift-off height using a burner feeding three streams of a central diluted methane jet surrounded by a coflowing lean metane-air jet and an outer coflowing air, and verified a lifted flame stabilized in downstream, which has a tribrachial flame structure consisting of a diffusion flame embedded within a inner fuel-rich and a outer fuel-lean premixed flame and merging at the leading edge of the flame called the triple point.

The burner consists of a central nozzle with a diameter of 2 mm surrounded by a tube with a diameter of 20 mm and a potential nozzle with an exit diameter of 150 mm. To save computational cost for calculation of the variable transport properties which is comparable to the cost for solutions of a set of ordinary differential equations, the diameter of the potential nozzle is assumed to be 70 mm and slip condition is imposed. A reaction mechanism based on 17 species and 51 elementary reaction steps[15] is employed for the simulation of this methane flame. The flame is ignited by a heat source with a peak temperature of 2000 K at 20 mm above the burner centerline. The numerical grid and boundary conditions for the mean velocities and mass fractions of the three streams are shown in Figure 5.

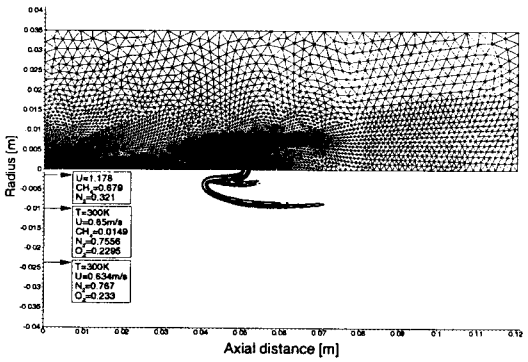


Figure 5 Unstructured grid and boundary conditions for lifted methane-air triple flame (npoin=9613, ncell=18895, nface=28178, nfa2=329).

For the velocity profiles of the fuel jet flow and the coflowing fuel-lean jet flow, a laminar fully developed tube flow and an annular flow were assumed, respectively and a comparison between measured and calculated radial profiles of the axial velocity at 4 mm above the burner is shown in Figure 6.

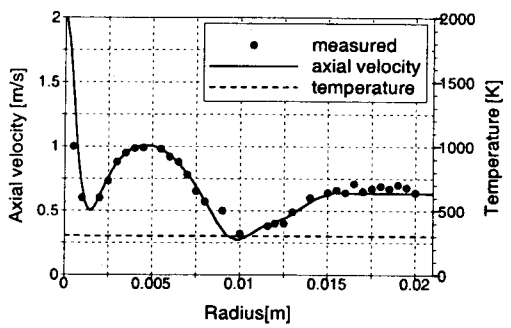


Figure 6 Calculated and measured radial profiles of axial velocity at 4.0mm above the burner.

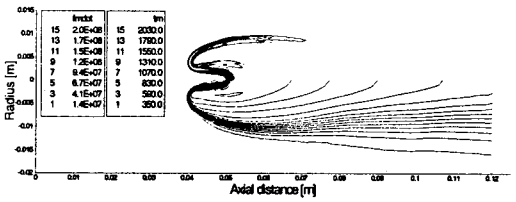


Figure 7 Predicted flame patterns in terms of heat release rate and temperature.

Figure 7 shows the predicted distributions of the heat release rate and temperature. The highest temperatures is found to be in the diffusion flame while the heat realease rate peaks around the leading edge of the triple flame. The maximum temperature of about 2036K and the stabilization height $h$ of about 39.9 mm above the burner are found from the simulation.

Figure 8 shows a comparison between measured and calculated profiles of the axial velocity along the constant radial position r=3.25 mm which pass through the triple point. It can be seen that the flow decreases immediately ahead of the flame with a radial divergence due to gas expansion and increases stongly at the flame front, and then the burnt gas has been accelerated further downstream.

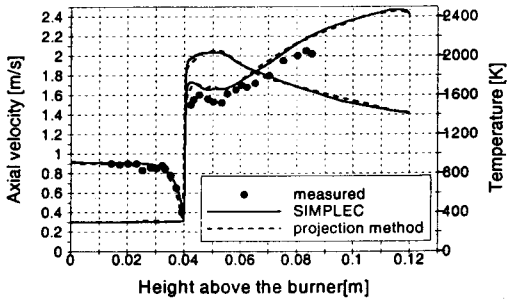


Figure 8 Comparison between measured and calculated profiles of the axial velocity along the constant radial position r=3.25 mm

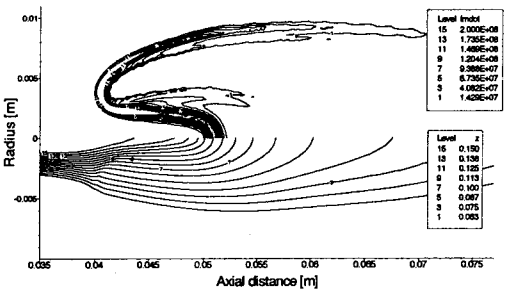


Figure 9 Contours of the mixture fraction distribution together with the heat release rate.

Figure 9 shows the calculated distribution of the mixture fraction together with the heat release rate.

## CONCLUSIONS

The unstructured-grid finite volume method has been developed to accurately resolve the physically and geometrically complex reacting flows. Numerical results indicate that the present model is quite capable of predicting the essential features and complex structure of the laminar nonpremixed and partially premixed flames. The extensions to the transient three-dimensional reacting flows and the multiphase flame field are currently under way.

## REFERENCES


1. Patankar, S.V., *Numerical Heat Transfer and Fluid Flow*, Hemisphere, Washington, D.C. (1980).
2. Van Doormaal, J,P. and Raithby, G.D., "Enhancement of the SIMPLE method for Predicting Incompressible Flows," *Numerical Heat Transfer*, vol. 7, pp. 147-163 (1984).
3. Chorin, A.J., "A Numerical Method for Solving Incompressible Viscous Flow Problems," *J. Computational Physics*, 2, 12-26 (1967).
4. Knio, O.M., Najm, H.N., and Wyckoff, P.S., "A Semi-implicit Numercal Scheme for Reacting Flow: II. Stiff, Operator-Split Formulation," *J. Comput. Physics*, 154, pp. 428-467 (1999).
5. Shang, H.M. and Chen, Y.S., "Unstructured Adaptive Grid Method for Reacting Flow Computation," AIAA 97-3183, 33rd AIAA/ASME/SAE/SAEE Joint Propulsion Conference & Exhibit (1997).
6. Kim, Y.M. and Kim, H.J., "Multidimensional Effects on Structure and Extinction Process of Counterflow Nonpremixed Hydrogen-Air Flames," *Combust. Sci. and Tech.*, vol. 137, pp. 51-80 (1998).
7. Trees, D., Brown, T.M., Seshadri, K., Smooke, M.D., Balakrishnan, G., Pitz, R.W., Giovangigli, V., and Nandula, S.P., "The Structure of Nonpremixed Hydrogen-Air Flames," *Combust. Sci. and Tech.*, vol. 104, pp. 427-439 (1995).
8. Plessing, T., Terhoeven, P., Peters, N., and Mansour, M.S., "An Experimental and Numerical Study of a Laminar Triple Flame," *Combustion and Flame*, 115:335-353 (1998).
9. Mathur, S.R. and Murthy, J.Y., "A Pressure-based Method for Unstructured Meshes," *Numerical Heat Transfer*, Part B, 31:195-215 (1997).
10. Rhie C.M. and Chow, W.L., "Numerical Study of the Turbulent Flow Past an Airfoil with Trailing Edge Separation," *AIAA J.* vol. 21, no. 11, pp. 1525-1532, November (1983).
11. Hoffmann, K.A. and Chiang, S.T., *Computational Fluid Dynamics for Engineers*, Engineering Education System, pp. 307 (1993).
12. Chase, M., *JANAF Thermodynamic Tables*, 3rd Ed., American Chemical Society and American Institute of Physics for the National Bureau of Standards (1986).
13. Kee, R.J., Warnatz, J., and Miller, J.A., Sandia Report, SAND83-8920 (1983).
14. Balakrishnan, G., Trees, D., and Williams, F.A., "An Experimental Investigation of Strain-induced Extinction of Diluted Hydrogen-air Counterflow Diffusion Flames," *Combust. and Flame*, 98, 123

(1994).
15. Djavdan, E., Darabiha, N., Giovangigli, V., and Candel, S.M., *Combust. Sci. and Tech.*, Vol. 76, pp. 287-309 (1991).